

Research Article

Transonic Flow of Moist Air around the ONERA M6 Wing with Non-equilibrium and Homogeneous Condensation

Sun Xiuling, Li Liang and Li Guojun

School of Energy and Power Engineering, Xi'an Jiaotong University, China

Abstract: A numerical investigation of the adiabatic and condensing flow field around the ONERA M6 wing is performed. The fundamental equations are based on the compressible Navier-Stokes equations and three additional conservation equations for the liquid phase. Homogeneous nucleation and non-equilibrium condensation are modelled by the classical condensation theory. The Harten's high-resolution TVD scheme is implemented for solving these equations. Three-dimensional transonic flows around the ONERA M6 wing under wind tunnel conditions are calculated by changing the relative humidity at three angles of attack, 1.07, 3.06 and 6.06 deg. The calculated results indicate that the onset of condensation is very sensitive to the angle of attack and the atmospheric humidity conditions. The condensation induces the release of latent heat and it directly affects the pressure coefficient distributions on the airfoil surface by increasing the humidity. Consequently, the lift-to-drag ratio of the airfoil is strongly influenced.

Keywords: Moist air, non-equilibrium condensation, transonic flow

INTRODUCTION

In transonic flow around an airplane wing in atmospheric flight, the combination of large expansion rates and moist air can cause significant changes in the lift and drag coefficients compared with dry air. Water vapor contained in moist air undergoes rapid expansion in the local supersonic region around a body. The high latent heat of water under a large acceleration can produce a super-saturated flow field and the onset of homogeneous condensation. The addition of latent heat to the flow field can remarkably alter the thermodynamic and flow properties. Typically, the condensation phenomena around airfoils moving at transonic speeds appear as the so-called 'vapor cloud'. Campbell *et al.* (1989) have summarised a number of natural condensation patterns. In their examples, the condensation process is observed in the taking off, landing and cruising of airplanes. It is also expected that the heat released by condensation to the surrounding flow field can affect the flow properties and the aerodynamic performance of the airplane. Studying the heat addition by condensation around airfoils is of fundamental interest and is useful for the design of airplane wings and helicopter blades.

The first experimental results concerning condensation phenomena in transonic flows around an airfoil were reported by Head (1949). Transonic flows over an airfoil in moist air were studied by Schnerr and Dohrmann (1990, 1994). The results were compared with the experimental Schlieren photographs. The results of the inviscid flow calculation also showed that

the airfoil performance, such as lift and drag, is strongly affected by relative humidity. Transonic viscous flows of moist air around the NACA0012 airfoil under atmospheric wind tunnel conditions were studied by Iriya *et al.* (1996) using classical condensation theory. A small disturbance model for the transonic flow of moist air with non-equilibrium condensation around a thin airfoil was presented by Rusak and Lee (2000). Three-dimensional subsonic flows over the 76° sharp-edged single-delta wing in an atmospheric wind tunnel under flight conditions were calculated by Yamamoto (2003). Homogeneous and heterogeneous condensation flow fields around a three-dimensional body in atmospheric flight were reported by Goodheart and Schnerr (2005). The humidity effects on the aerodynamic characteristics of an airplane model were investigated by Jordan (1989).

The purpose of the present study is to apply computational codes by Li *et al.* (2005) to transonic viscous flows around the ONERA M6 wing under atmospheric wind tunnel conditions. The performance of the airfoil under these conditions is predicted by changing the relative humidity at three angles of attack, 1.07, 3.06 and 6.06 deg. The condensation cloud around the wing is captured and the pressure drag, lift and lift-to-drag ratio are also evaluated.

MATHEMATICAL MODEL

The condensing flow of moist air can be regarded as a two-phase system. The primary phase is the

gaseous phase, which consists of dry air and water vapor, while the secondary phase is the liquid phase, which consists of a large number of condensed water droplets. A homogeneous condensation flow without inter-phase velocity slip between the moist air and water droplets is assumed as the radii of the water droplets are sufficiently small. Thus, an Eulerian-Eulerian model can be established. The conservation of mass, momentum and energy equations for the gaseous phase are written as:

$$\frac{\partial \rho_g}{\partial t} + \frac{\partial (\rho_g u_j)}{\partial x_j} = -\rho \dot{m} \quad (1)$$

$$\frac{\partial (\rho_g u_i)}{\partial t} + \frac{\partial (\rho_g u_i u_j)}{\partial x_j} = -\frac{\partial p}{\partial x_i} + \frac{\partial \tau_{ij}}{\partial x_j} - \rho \dot{m} u_i \quad (2)$$

$$\frac{\partial (\rho_g E_g)}{\partial t} + \frac{\partial (\rho_g E_g u_j)}{\partial x_j} = \frac{\partial (p u_j)}{\partial x_j} + \frac{\partial (u_i \tau_{ij} - q_j)}{\partial x_j} - \dot{m} (h_t - h_{fg}) \quad (3)$$

Here, the source terms $-\rho \dot{m}$, $-\rho \dot{m} u_i$ and $-\rho \dot{m} h_t$ are introduced to count the mass, momentum and energy interactions, respectively, between the gaseous and the liquid phases. The condensation mass rate \dot{m} is given by:

$$\dot{m} = (1-Y) \rho_l J \frac{4\pi r_c^3}{3} + 4\pi r^2 \frac{dr}{dt} \rho_l N \quad (4)$$

Here, the nucleation rate J and droplet growth rate dr/dt are determined using the classical nucleation theory and the same expressions used by Guha and Young (1991) are adopted.

As mentioned above, the velocity slip between the two phases can be neglected. Therefore, the condensate droplets have the same velocity field as the gaseous phase. The conservation laws for water vapor density, water droplet number density N and condensate mass fraction Y can be written as:

$$\frac{\partial \rho_v}{\partial t} + \frac{\partial (\rho_v u_j)}{\partial x_j} = -\rho \dot{m} \quad (5)$$

$$\frac{\partial \rho N}{\partial t} + \frac{\partial (\rho N u_j)}{\partial x_j} = \rho_g J \quad (6)$$

$$\frac{\partial \rho Y}{\partial t} + \frac{\partial (\rho Y u_j)}{\partial x_j} = \rho \dot{m} \quad (7)$$

Based on the condensate mass fraction Y and water droplet number density N , the water droplet radius can be calculated from:

$$r = \sqrt[3]{3Y / (4\pi \rho_l N)} \quad (8)$$

As the condensate mass fraction is sufficiently small, the state equation for moist air is given by:

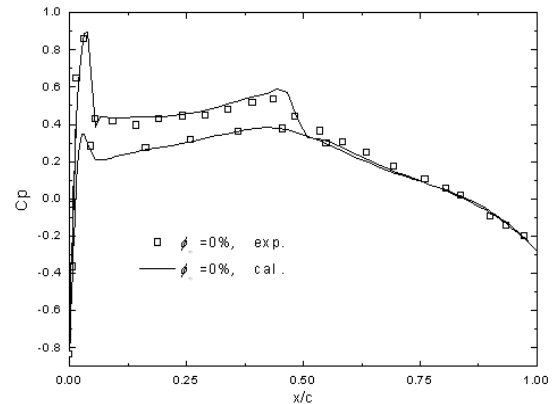
$$p = \rho_g RT \quad (9)$$

Therefore, with Eq. (1, 3, 5 and (9)), the moist air flow with condensation can be solved. The high-resolution finite-difference method and the explicit time-marching technique are adopted. The second-order upwind scheme is used in the spatial discretisation.

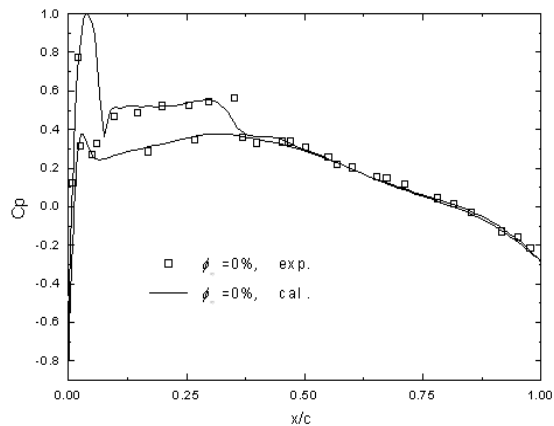
Some calculations were executed to check the reliability of the present model and numerical method. Transonic flow around the NACA 0012 airfoil was calculated by Li *et al.* (2005). Non-equilibrium condensation and condensation shock are captured in the calculation. The pressure coefficient and the normal shock agree well with the results presented by Schnerr and Dohrmann (1990).

NUMERICAL RESULTS

Adiabatic verification: The classical test case of the ONERA M6 wing is used to examine the effects of

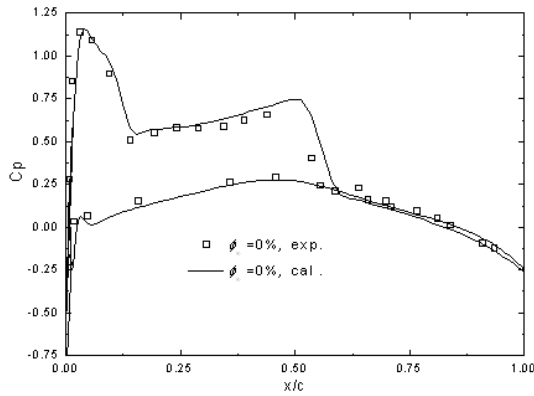


(a)

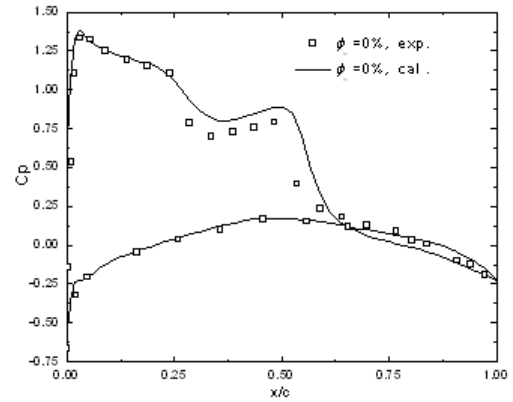


(b)

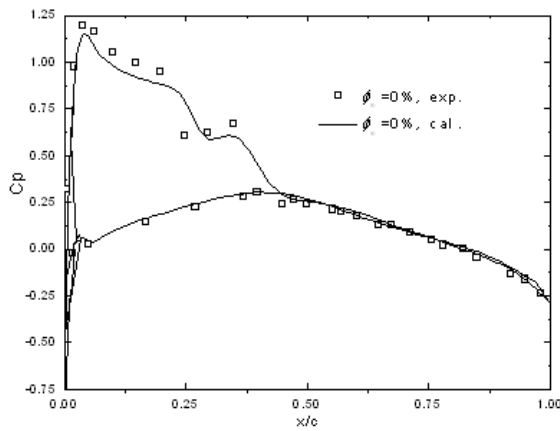
Fig. 1: ONERA M6 adiabatic pressure coefficient for an angle of attack of 1.07 deg compared with experimental results; (a) 44% span; (b) 80%



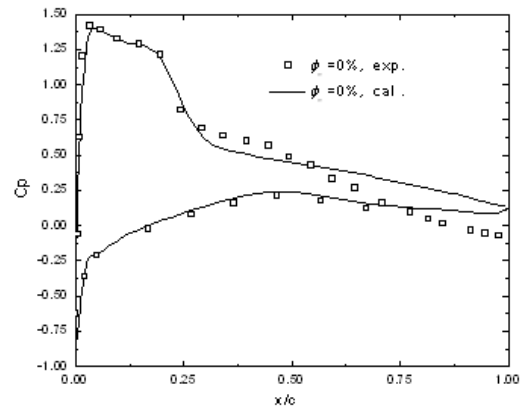
(a)



(a)



(b)



(b)

Fig. 2: ONERA M6 adiabatic pressure coefficient for an angle of attack of 3.06 deg compared with experimental results; (a) 44%; (b) 80% span

Fig. 3: ONERA M6 adiabatic pressure coefficient for an angle of attack of 6.06 deg compared with experimental results; (a) 44%; (b) 80% span

condensation because of the available geometry and adiabatic pressure data by Schmitt and Charpin (1979). The ONERA M6 is a swept-back wing with zero twist and nobody fillets or strakes. The mean chord length of the wing is 0.646 m, which is the same length as the original experiment in the wind tunnel. Atmospheric wind tunnel conditions are assumed. For all the calculations, the flow conditions are specified such that the free-stream Mach number is 0.84, the free-stream temperature is 293.15 K and the free-stream pressure is 1.0×10^5 Pa. The grid number was approximately 350,000. Before beginning with the condensation results, a comparison is made between adiabatic experiments and the calculations at various angles of attack. Figure 1 to 3 show the comparisons of two different pressure coefficients at 44 and 80% of the wing span for angles of attack of 1.07, 3.06 and 6.06 deg, respectively. The numerically predicted results are in good agreement with the experimental measurements. For the lower angle of attack of 1.07 deg, there is a weaker second shock and the position

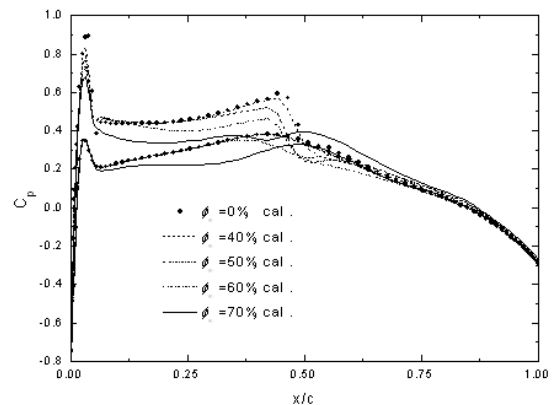


Fig. 4: ONERA M6 pressure coefficient for different humidity values at an angle of attack of 1.07 deg at 44% span

and strength of the shock agree well with the results of the experiments. For a larger angle of attack of 3.06 deg, the double shock system is present at 44 and 80%

Table 1: The lift, pressure drag coefficients and lift/drag ratio for different relative humidity values

ϕ_c	30%	40%	50%	60%	70%
$(c_{L,\phi>0}-c_{L,\phi=0})/c_{L,\phi=0} \times 100$	-1.38	-6.74	-14.72	-16.81	-17.44
$(c_{D,\phi>0}-c_{D,\phi=0})/c_{D,\phi=0} \times 100$	11.84	17.44	44.29	119.78	191.68

span. For an angle of attack of 6.06 deg, the double shock system is present near the root of the wing. However, moving to the tip at 80% wing span, see Fig. 3b, a separation zone is observed from the C_p data and the separation point is accurately captured. The recovery pressure is high at the leading edge and then decreases as it reaches the trailing edge.

Non-adiabatic flows: For all of the following test cases, the relative humidity is set from 30% to 70%. The free-stream Mach number, free-stream temperature and free-stream pressure were chosen to be the same values as in the adiabatic experiments.

The first set of results compares the effect of changing the relative humidity while keeping the angle of attack at 1.07 deg. Table 1 shows that the lift decreases and the pressure drag increases as the humidity increases. By examining the C_p plots, one can see where this decrease or increase comes from. Figure 4 compares the changes in C_p due to various levels of relative humidity at 44% wing span. The results on the upper surface are especially important for the present study.

The increase of the pressure due to condensation with increases in the relative humidity is clearly observed at the upper surface. In the C_p plots,

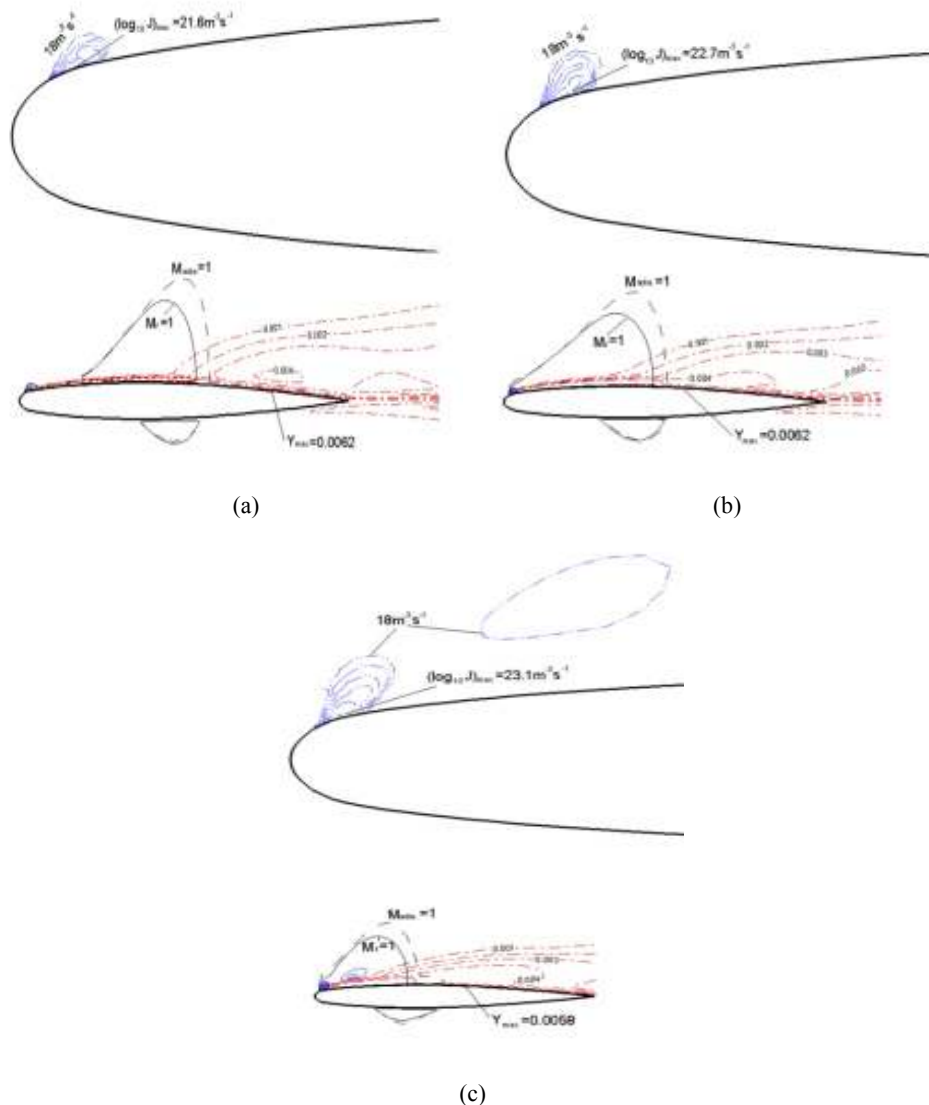


Fig. 5: Condensation mass fraction Y , log nucleation rate and sonic line at an angle of attack of 1.07 deg at a relative humidity of 50%; (a) 20% wing span; (b) 44% wing span; (c) 80% wing span

30% relative humidity with a small amount of water vapor was not graphed because it follows the same trend as adiabatic flow. Leaving this data series out makes the graph less crowded.

At a relative humidity of 40%, there is a small decrease in C_p at the leading edge, which increases drag, while the position of the second shock is unchanged. The reason for this is that the humidity is lower and a small quantity of the water vapor contained in moist air and the large acceleration at the leading edge causes a small amount of homogeneous condensation.

At a relative humidity of 50%, a decrease in C_p occurs at the leading edge. The second shock shifts upstream towards the leading edge on the suction surface, which decrease lift. Note that the supersonic region is decreased. The overall change is a decrease in lift and an increase in drag.

At a relative humidity of 60%, a larger decrease in C_p occurs at the leading edge and the second shock continues to shift upstream towards the leading edge on the suction surface with increasing the humidity. Note

that the pressure is a little higher before the second shock, which decreases the lift; also, the supersonic region is decreased, which decreases the lift. A small increase of pressure towards the trailing edge on the pressure side is observed, which increases the lift. Therefore, balance is observed.

When the relative humidity reaches 70%, the second shock becomes weaker and the static pressure is higher on the suction surface. Additionally, a decrease of C_p occurs on the pressure side. The increase of the static pressure on the pressure side has the effect of increasing lift. The drag is also significantly increased on the leading edge by the heat addition. The overall change is a substantial decrease in lift and increase in drag.

Figure 5 shows the condensation mass fraction Y , the log nucleation rate and the adiabatic/condensing sonic line at 20, 44 and 80% wing span at a relative humidity of 50%. The region where water droplets occur spreads wider at the suction surface of the wing than that at the pressure surface, which causes the changes in C_p . The effect of

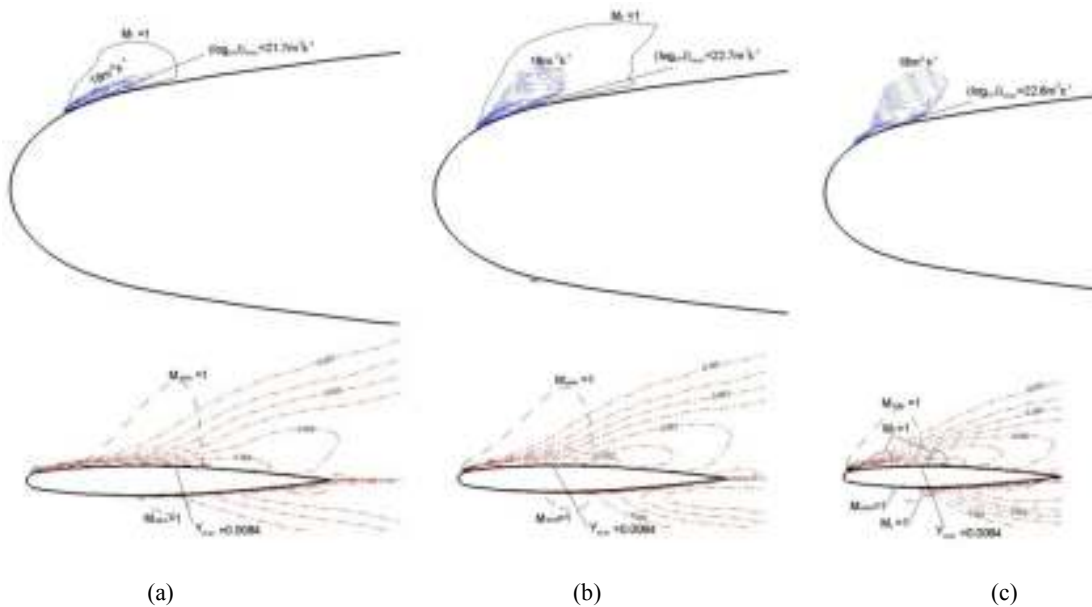


Fig. 6: Condensation mass fraction Y , log nucleation rate and sonic line at an angle of attack of 1.07 deg at a relative humidity of 70%; (a) 20% wing span; (b) 44% wing span; (c) 80% wing span

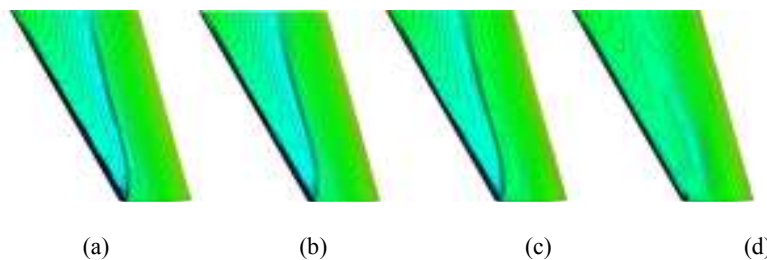


Fig. 7: ONERA M6 wing top pressure distribution at an angle of attack of 1.07 deg; (a) $\phi_\infty = 0\%$; (b) $\phi_\infty = 30\%$; (c) $\phi_\infty = 50\%$; (d) $\phi_\infty = 70\%$

condensation becomes much stronger from the root to the wing tip (Fig. 5). The maximum of the log nucleation rate is approximately 21.7 at 20% wing span; however, it reaches 23.1 at 80% wing span. Figure 6 shows the condensation mass fraction Y , the log nucleation rate and the adiabatic/condensing sonic line at 20, 44 and 80% wing spans at a relative humidity of 70%. In Fig. 6, the effect of condensation over the wing span from root to tip follows the same trend as at 50% relative humidity. An interesting result at 70% relative humidity is that the size of the supersonic

region decreases sharply. At 20 and 44% wing span, the supersonic region shrinks acutely on the suction surface; however, it disappears on the pressure surface. At 80% wing span, the area of the supersonic region also decreases on the suction surface, while it decreases and shifts downstream on the pressure surface. As the relative humidity is increased, a large number of water droplets occur, which release a significant quantity of heat to the flow field. These changes sharply increase the static pressure and lower the pre-shock Mach number on part of the wing. Figure 7 shows the wing

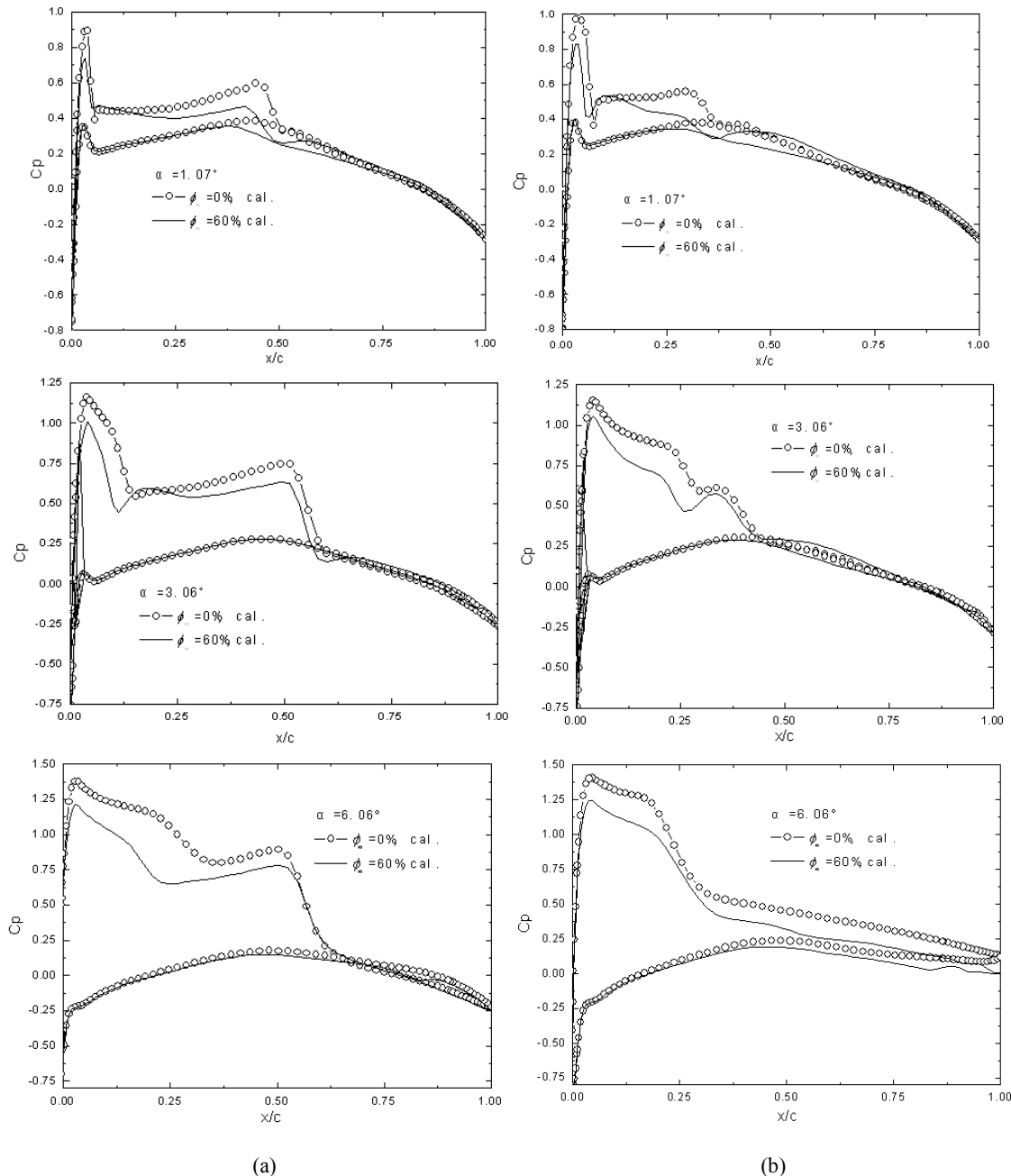


Fig. 8: ONERA M6 wing pressure coefficients of adiabatic flow and condensing flow cases for different angles of attack; (a) 44% wing span; (b) 80% wing span

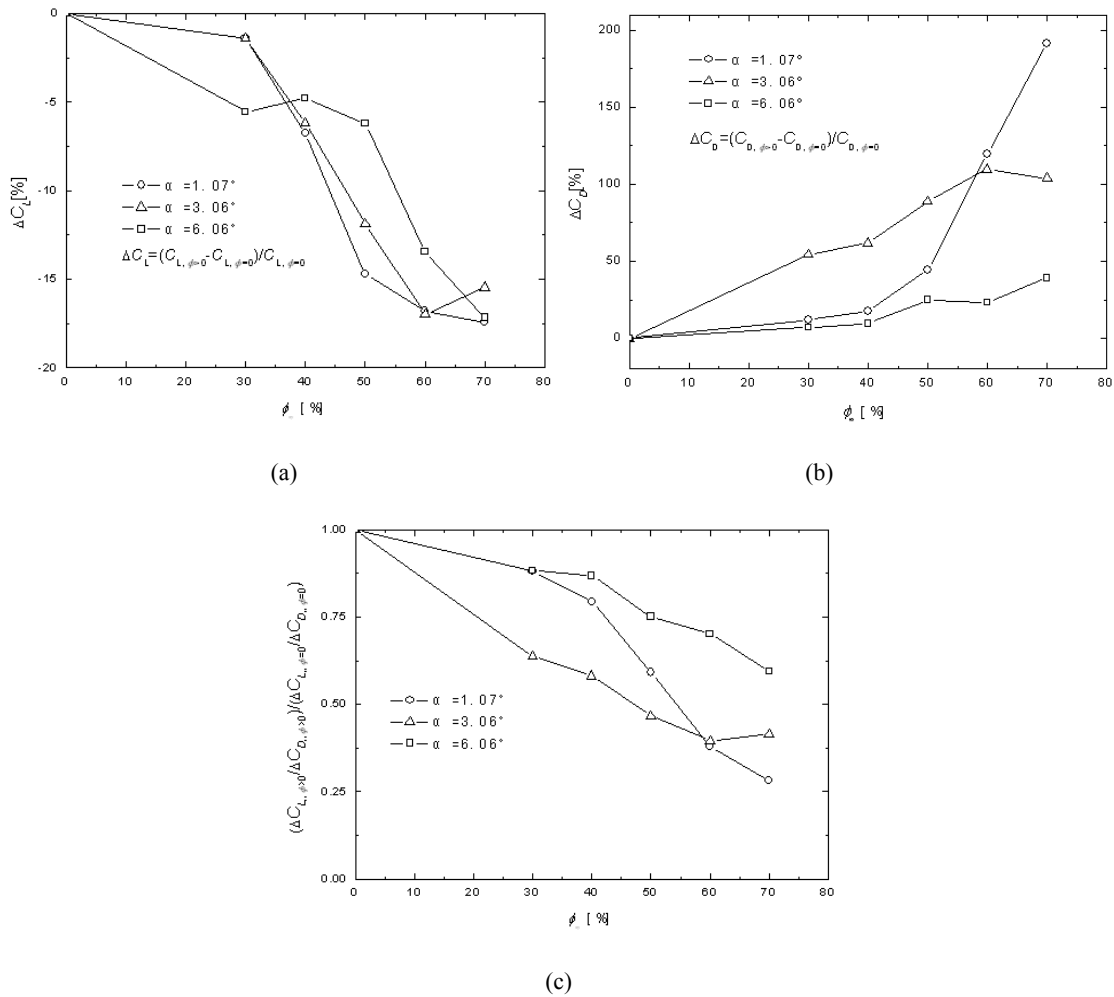


Fig. 9: ONERA M6 wing lift, drag and lift-to-drag ratio as a function of humidity for different angles of attack; (a) Lift coefficient; (b) Pressure drag coefficient; (c) Lift-to-drag ratio

top pressure distribution for the adiabatic case and homogeneous condensation. As shown in Fig. 7, the second shock is considerably weakened at 70% relative humidity.

To investigate the effect of how lift and pressure drag coefficients are affected due to homogeneous condensation at various angles of attack, Fig. 8 shows the pressure coefficient at 44% and 80% wing span for the adiabatic and condensing flow ($\phi_\infty = 60\%$) cases with varying angles of attack. For all angles of attack, the supersonic region is reduced due to homogeneous condensation occurring and there is a decrease in C_p at the leading edge. The position of the second shock shifts towards the leading edge on the suction surface for angles of attack of 1.07 deg and 3.06 deg. In addition, at a higher angle of attack of 6.06 deg, the second shock position on the suction surface is unchanged due to condensation being produced only at the leading edge, which is why there is a much larger static pressure increase at the leading edge compared with the earlier two angles. This effect is due to fast expansions with higher angles of attack.

The final analysis involves the change in lift and pressure drag and the lift-to-drag ratio in Fig. 9, which is used to compare the effects of homogeneous condensation at varying angles of attack. For all the angles of attack, the lift and the lift-to-drag ratio decrease rapidly with an increase in the relative humidity under the present atmospheric wind tunnel conditions and the pressure drag increases with increases in the humidity. In Fig. 9b, the pressure drag coefficient shows the largest increase with the smallest angle of attack; the largest increase in drag reaches 191% at an angle of attack of 1.07 deg at a relative humidity 70%. The pressure drag coefficient for the highest angle of attack of 6.06 deg shows a relatively small increase, which is partially dominated by the separation occurring near the tip. As the water vapor contained in moist air is increased, the latent heat increases. When latent heat is added to the flow, it has the effect of reducing the separation region, which decreases the drag, but the drag is increased due to the heat addition at the leading edge. Therefore, balance is

observed. As shown in Fig. 8, the separate region is decreased.

CONCLUSION

An Eulerian-Eulerian model has been applied to investigate moist air flow with non-equilibrium condensation. Based on this model, three-dimensional transonic viscous flows over the ONERA M6 wing under atmospheric wind tunnel conditions were calculated. The relative humidity is changed to see their effects due to homogeneous condensation at three angles of attack of 1.07, 3.06 and 6.06 deg. The calculated results indicate that the condensation strongly depends on atmospheric humidity conditions and the angle of attack. For all three angles of attack, the effect of condensation becomes much stronger at the span from the root to the wing tip and the pressure increases on the suction surface due to the release of latent heat with non-equilibrium condensation at any fixed relative humidity. The lift is decreasing and the lift-to-drag ratio becomes small as the relative humidity increases. The pressure drag shows a different trend with increasing humidity. The pressure drag change with the humidity presents the largest increase with the smallest angle of attack of 1.07 deg and a relatively small increase is observed for the largest angle of attack of 6.06 deg.

The present study mainly investigated the effect of non-equilibrium condensation under atmospheric wind tunnel conditions. However, actual flight conditions, including the altitude, length scale, particle density, particle radius and condensation pattern, are not always the same as wind tunnel conditions. Further study should be conducted to improve the present method for calculating condensation in actual flight conditions under different conditions.

Notation:

c : Chord length of airfoil
 C_D : Pressure drag coefficient
 C_L : Lift coefficient
 C_p : Specific heat at const pressure; pressure coefficient
 d : Humidity
 E : Total specific internal energy of moist air
 f : Frequency
 h_{fg} : Latent heat
 h_t : Total specific enthalpy of moist air
 J : Nucleation rate
 L : Latent heat
 $\rho\dot{m}$: Condensate mass rate per unit mass of moist air mixture
 M_a : Mach number
 N : Number of droplets
 p : Pressure of moist air
 q_j : Heat flux in the j th coordinate direction

r : Radius of water droplet
 r_c : Kelvin-Helmholtz critical radius
 R : Gas constant of moist air mixture
 t : Time
 T : Temperature
 u_i, u_j : Velocity component
 x_i, x_j : Spatial coordinate
 Y : Condensate mass fraction
 ρ : Density of moist air and water droplet mixture
 ρ_g : Density of gaseous phase
 ρ_l : Density of liquid water
 ρ_v : Density of water vapour
 τ_{ij} : Viscous stress
 ϕ : Relative humidity

Subscripts

0: Stagnation condition
 ∞ : Far-field condition
 adia: Adiabatic flow
 f: Nonadiabatic flow.

REFERENCES

- Campbell, J.F., J.R. Chambers and C.L. Rumsey, 1989. Observation of airplane flow fields by natural condensation. *J. Airc.*, 26(7): 593-605.
- Goodheart, K.A. and G.H. Schnerr, 2005. Condensation on ONERA M6 and F-16 wings in atmospheric flight: numerical modelling. *J. Airc.*, 42(2): 402-412.
- Guha, A. and J.B. Young, 1991. Time-marching prediction of unsteady condensation phenomena due to supercritical heat addition. *Proceeding of Conference Turbomachinery: Latest Developments in a Changing Scene*. IMechE Paper C423/057, pp: 167-177.
- Head, R.M., 1949. Investigations of spontaneous condensation phenomena. Ph.D. Thesis, California Institute of Technology, Pasadena, CA.
- Iriya, A., S. Yamamoto and H. Daiguji, 1996. Numerical method for transonic viscous flow considering humidity. *Trans. Jpn. Soc. Mech. Eng.* (in Japanese), 62: 100-105.
- Jordan, F.L., 1989. Investigation at near-sonic speed of some effects of humidity on the longitudinal aerodynamic characteristics of a NASA supercritical wing research airplane model. NASA TMX-2618.
- Li, L., X.L. Sun, Z.P. FENG and G.J. Li, 2005. Transonic flow of moist air around a NACA0012 airfoil with non-equilibrium condensation. *Proc. Nat. Sci.*, 15(9): 838-842.
- Rusak, Z. and J.C. Lee, 2000. Transonic flow of moist air around a thin airfoil with non-equilibrium and homogeneous condensation. *J. Fluid Mech.*, 403: 173-199.

- Schmitt, V. and F. Charpin, 1979. Pressure distributions on the ONERA M6 wing at transonic Mach numbers. Experimental data base for computer program assessment. Report of the Fluid Dynamics Panel Working Group 04, AGARD AR 138.
- Schnerr, G.H. and U. Dohrmann, 1990. Transonic flow around airfoils with relaxation and energy supply by homogeneous condensation. *AIAA J.*, 28(7): 1187-1193.
- Schnerr, G.H. and U. Dohrmann, 1994. Drag and lift in nonadiabatic transonic flow. *AIAA J.*, 32(1): 101-107.
- Yamamoto, S., 2003. Onset of condensation in vortical flow over sharp-edged delta wing. *AIAA J.*, 41(9): 1832-1842.